CHALLENGES IN EUROPEAN AEROSPACE
5TH CEAS AIR & SPACE CONFERENCE

CEAS

APIAN-INF: a Low-Speed Aerodynamic and Aeroacoustic Investigation of Pylon – Pusher Propeller Interaction Effects

Tomas Sinnige[1], Anwar M. N. Malgoezar, Daniele Ragni, Kirk Y. W. Scheper, Mirjam Snellen, Georg Eitelberg, Leo L. M. Veldhuis

Delft University of Technology, Faculty of Aerospace Engineering, Kluyverweg 1, 2629 HS, Delft, the Netherlands

ABSTRACT

An experimental investigation was performed at the Large Low-speed Facility of the German-Dutch wind tunnels (DNW-LLF) to study the pylon interactions associated with pusher propellers. The aerodynamic and aeroacoustic effects of pylon trailing edge blowing and swirl recovery vanes (SRVs) were evaluated. The pylon installation increased the summed tonal noise levels by up to 13 dB in unblown conditions, while the propulsive performance was affected in asymmetric inflow conditions only. At a sideslip angle of +6°, pre-swirl of the flow due to the pylon tip vortex led to a thrust increase of 10% at high thrust up to 45% at a low thrust setting. Stereoscopic PIV measurements showed the beneficial effect of pylon blowing in compensating the momentum deficit in the pylon wake. At the optimal blowing rate, a recovery effect of about 80% was obtained compared to the unblown case. Application of the blowing system eliminated the pylon installation penalty, recovering the noise levels to those measured for the isolated propeller. Installation of the SRVs downstream of the isolated propeller resulted in a swirl recovery of 50%, at the cost of a 2 dB tonal noise increase.

1 INTRODUCTION

Due to advancements in aerodynamic and aeroacoustic design, material technology, and manufacturing processes, modern propellers provide an interesting alternative to turbofans. While becoming more competitive in terms of maximum operating speed and specific thrust, propellers offer a higher propulsive efficiency because of their larger effective by-pass ratio. The corresponding reduction in specific fuel consumption is the main motivation for today's research on propellers. Driven by interior noise considerations, propeller aircraft lay-outs with rear-fuselage mounted contra-rotating open rotors (CRORs) are most often studied.[1] However, in such a configuration the propeller blades pass through the wake of the upstream pylon. This results in unsteady blade loads, and associated increased propeller noise emissions.[2] Studies with CRORs showed that these installation effects are dominated by the interaction between the pylon wake and the front rotor.[2-5]

Pylon blowing can be used to compensate the momentum deficit in the pylon wake, thereby mitigating the pylon installation effects. This has been confirmed by previous studies focusing on single-rotating[6,7] and contra-rotating[3-5,8,9] propellers. However, as of now no comprehensive data set dealing with the pylon wake interactions is available in the public domain. The present research aims at quantifying the performance and noise penalties resulting from the pylon – pusher propeller interactions, including the effects of pylon trailing edge blowing. Performed in the EU-funded ESWIRP project, the study named APIAN-INF involved contributions from Airbus, Delft University of Technology, DLR, DNW, INCAS, TsAGI, TU Braunschweig, and the University of Cambridge.

To increase the propulsive efficiency of single-rotating propellers, swirl recovery vanes (SRVs) can be installed to reduce the swirl losses in the propeller slipstream. Similarly as for contra-rotating propellers, the installation of the swirl recovery vanes can increase the propulsive efficiency by converting the swirl in the propeller slipstream into an additional thrust component. However, compared to contra-rotating solutions, installation of the SRVs adds less complexity to the propulsion system because of the lack of a second rotating blade row. Previous research by NASA confirmed the potential of the SRVs to increase the propulsive efficiency, with measured efficiency gains of around

[1] *Corresponding author, PhD student, T.Sinnige@tudelft.nl*

two percent in cruise conditions.[10] Compared to an isolated propeller configuration without the SRVs installed, no additional noise was measured.[11] Considering the potential benefits of a propulsion system consisting of a single-rotating propeller with downstream SRVs, a preliminary assessment of the aerodynamic and aeroacoustic performance of such a combination was performed as a secondary part of the experiment treated in this paper.

2 EXPERIMENTAL METHODOLOGY

2.1 Wind Tunnel Facility and Models

The test campaign was performed at the Large Low-speed Facility of the German-Dutch wind tunnels (DNW-LLF). In the selected open jet configuration, the wind tunnel with outlet of 8 m x 6 m allows a wind speed range of 0 – 80 m/s. The turbulence level of the tunnel flow is less than 0.02%, while total pressure deviations are smaller than 0.1% at the position of the model. An installed pusher propeller configuration was simulated by positioning a powered propeller model downstream of a pylon equipped with a trailing edge blowing system. Tests were performed with and without the presence of the pylon, while the isolated propeller measurements were also done with swirl recovery vanes installed. A fixed support structure provided yaw control of the entire setup. A photograph of the propeller setup and measurement equipment used is depicted in Figure 1.

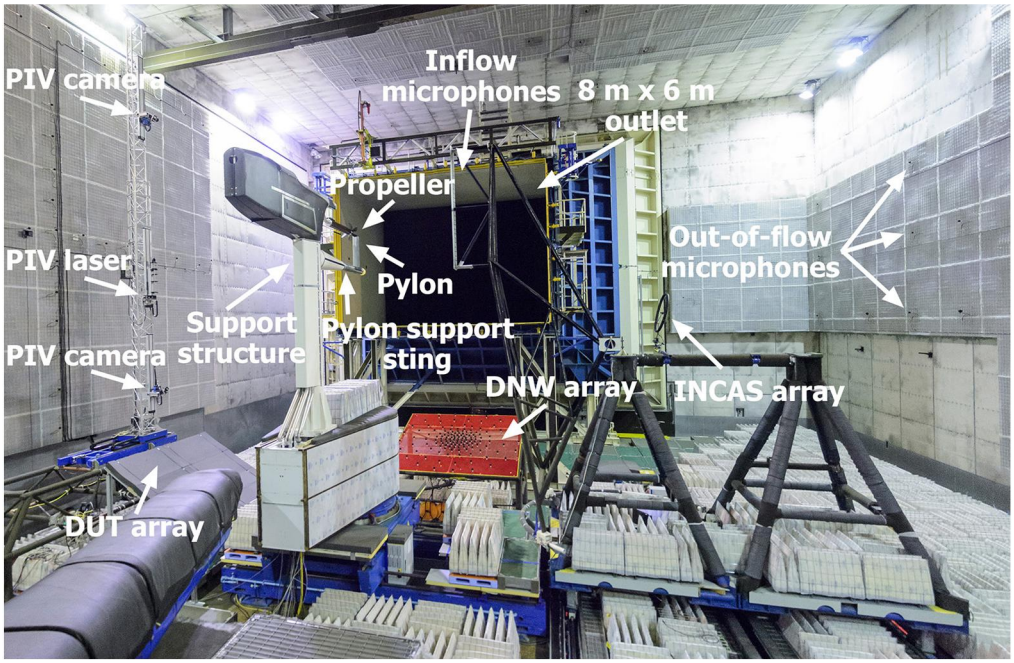

Figure 1: Overview of the test setup, showing models and the measurement equipment.

The six-bladed propeller model (Figure 2), designed and built for the European APIAN (Advanced Propulsion Integration Aerodynamics and Noise)[12,13] project, has a diameter of 0.508 m. The blade pitch angle at 75% of the radius was set to 40.4°.

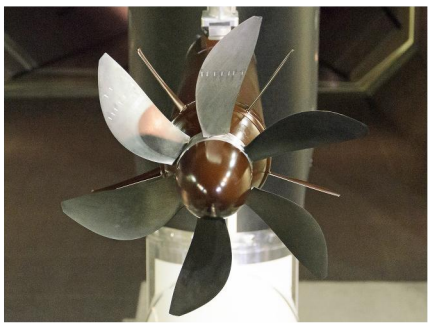

Figure 2: Propeller model.

The pylon model (Figure 3) was manufactured by extrusion of a NACA0010 profile into a straight wing of 0.9 m span and 0.489 m chord. The trailing edge thickness was modified to 0.8% of the chord to allow for the installation of the blowing system. The pylon was mounted upstream of the propeller

using a secondary sting, attached to the same support structure holding the propeller. This sting was not removed during measurements without the pylon.

The blowing system, installed in the aft part of the pylon, was designed following the Uniform Blowing Rod concept.[7] As opposed to choked systems, the uniformity of its outflow is governed by the shape of the blowing channel. The final geometry resulted in uniform outflow for spanwise locations upstream of the outboard part of the blade, with total pressure variations smaller than 5%. To cover the entire blade during the wake passage, the length of the blowing slit equaled 1.15 times the propeller radius. The flow rate supplied by the blowing system to the surrounding flow was monitored and regulated by a mass flow controller. A pylon blowing mass flow coefficient $c_{\dot{m}}$ is introduced as the ratio between the blown and freestream mass flows. The latter was referenced to the outflow area of the blowing slit.

Swirl recovery vanes were installed downstream of the isolated propeller to assess their potential to increase the system's propulsive efficiency. Five vanes were used, with a diameter equal to 90% of the rotor diameter to prevent tip vortex interaction noise. The vane design was obtained using a low-order design tool, based on the propeller analysis and design program XROTOR[14]. A side view of the propeller with swirl recovery vanes installed is given in Figure 4.

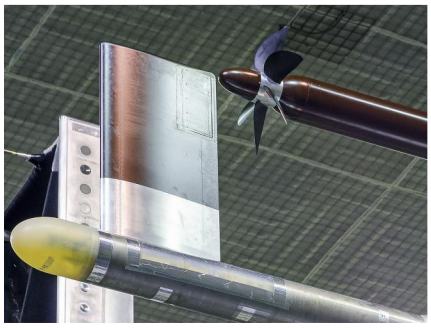

Figure 3: Pylon model.

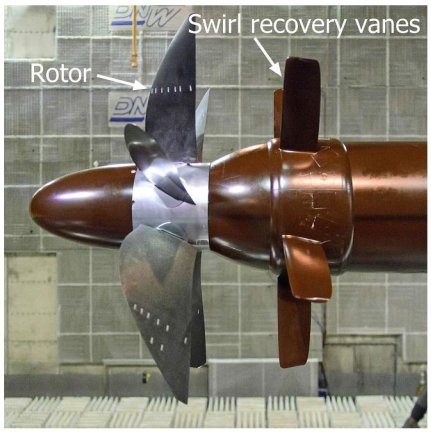

Figure 4: Propeller with swirl recovery vanes installed.

2.2 Measurement Techniques

The propulsive performance of the propeller model was monitored using a three-spoke, six-component rotating shaft balance (RSB). The thrust and torque were measured directly, while the other forces and moments followed from a decomposition of the two recorded in-plane components.

A stereoscopic PIV setup was prepared to quantify the momentum deficit in the pylon wake, with and without pylon blowing. The fields of view were positioned downstream of the pylon trailing edge, at six different vertical positions. To quantify the swirl recovery potential of the SRVs, the measurement plane was moved to encompass the propeller slipstream, at the vertical position of the propeller axis. The positions of all measurement planes are indicated in Figure 5.

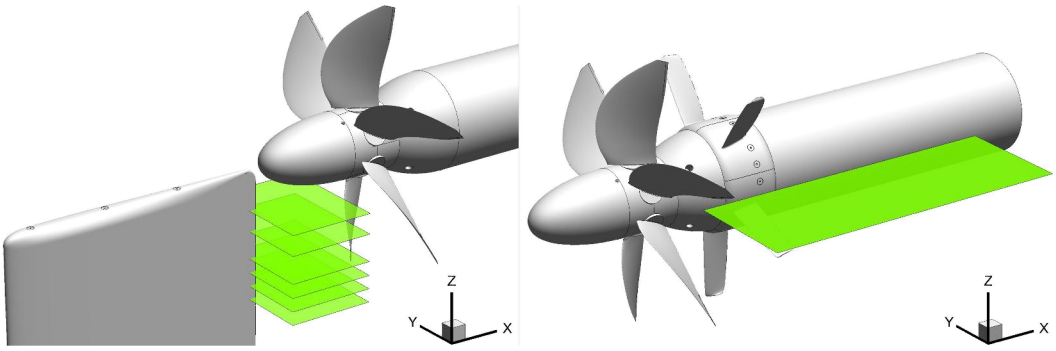

Figure 5: PIV measurement planes (green) in the pylon wake (left) and propeller slipstream (right) regions.

To quantify the impact of the installation of the pylon and SRVs on the propeller noise emissions, inflow and out-of-flow acoustic instrumentation were used. All results presented in this paper were obtained using the inflow microphones, provided by Airbus. The system consists of 39 microphones, integrated in the wing shaped structure depicted in Figure 6. A detailed description of the system is provided in Ref. [5]. The complete structure was traversed through the test hall in axial direction to cover an axial directivity angle range of $30° \leq \theta_e \leq 145°$, at a circumferential directivity range of $-26° \leq \phi \leq 26°$. The definition of the directivity angles θ and ϕ is provided in Figure 7. Throughout the paper the emission angles are used, not the geometric angles.

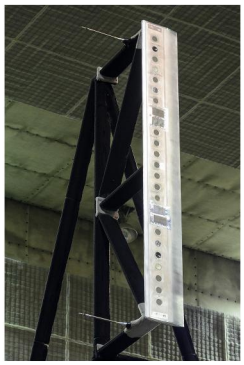

Figure 6: Traversable inflow acoustic instrumentation.

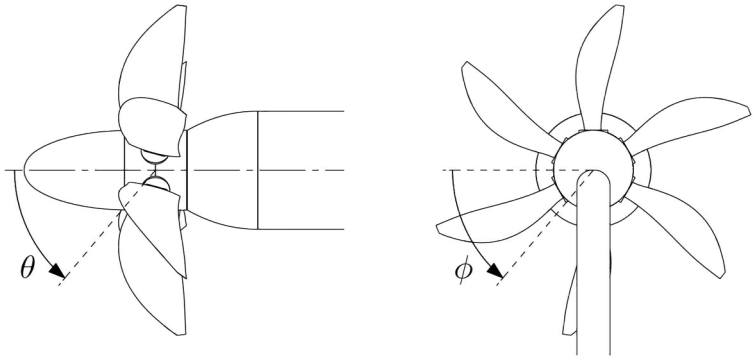

Figure 7: Definition of axial and circumferential directivity angles θ and ϕ.

Apart from the local measurements done with the inflow microphones, noise source localization was performed by employment of three acoustic arrays. The default DNW array was used, together with a custom-made array designed and built by Delft University of Technology (DUT), and an array operated by INCAS. Photographs of the three arrays are presented in Figure 8.

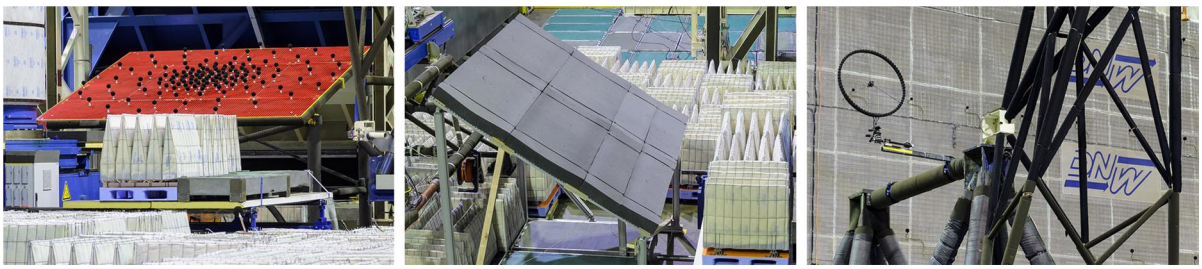

Figure 8: Microphone arrays from DNW (left), DUT (center), and INCAS (right).

The DNW array measures 4 m x 4 m and contains 140 microphones, and was placed upstream of the propeller. The DUT array has dimensions of 4 m x 3 m with a total of 63 microphones and was positioned approximately in the propeller plane, at a circumferential directivity angle of around 125 degrees. Finally, the INCAS array features a circular shape with a diameter of 1 m, and 72 microphones in total. The results presented in this paper were all measured using the DUT array. Conventional beamforming[15] was used to process the acquired data, in a plane parallel to the array plane at a distance of 8.1 m. The performance of the acoustic arrays was evaluated using a loudspeaker installed in a fairing in the flow, emitting white noise in the octave bands with center frequencies of 1 kHz and 2 kHz. Figure 9 presents the source map obtained using the DUT array, as measured at a freestream velocity of 60 m/s. Beamforming was applied for the frequency range of 1,500 Hz up to 2,000 Hz.

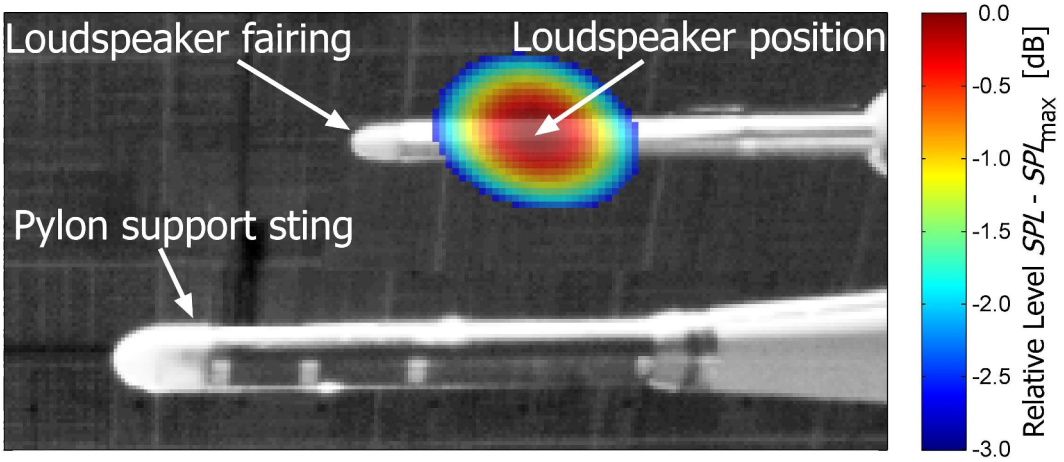

Figure 9: Sound source localization of calibration loudspeaker source with DUT array; U_∞ = 60 m/s, 1,500 Hz < f < 2,000 Hz.

The source map depicted in Figure 9 shows a single, clearly defined noise peak, as expected. The offset between the computed and true positions of the loudspeaker in the photo overlay was compensated for by shifting the photo. This shift was used to calibrate all results obtained from the DUT array.

2.3 Measurement Cases

To assess the sensitivity of the propeller performance and noise emissions to the advance ratio, sideslip angle, and pylon blowing coefficient, the measurements were performed at different operating conditions. An overview of the analyzed test cases is provided in Table 1.

Table 1: Overview of the analyzed test cases.

Parameter	Symbol	Value
Freestream velocity	U_∞	60 m/s
Propeller advance ratio	J	1.05, 1.40, 1.75
Angle of attack	α	0°
Angle of sideslip	β	0°, +6°, −6°
Pylon blowing coefficient	$c_{\dot{m}}$	0.0, 1.4, 1.6, 1.8

The selected advance ratios (J = 1.05, 1.40, 1.75) correspond to a "high", "medium", and "low" propeller thrust setting. The effect of asymmetric inflow was analyzed by performing measurements at 0° and ±6° of sideslip angle, as defined in Figure 10. The pylon blowing coefficients were selected based on tests performed before the start of the final measurement program. The noise emissions were recorded using the out-of-flow microphones for a range of blowing coefficients at a constant propeller operating point (J = 1.40, β = 0°). The blowing coefficient leading to the largest noise reductions ($c_{\dot{m}} = 1.6$) was selected for the final test program, together with coefficients equal to 85% and 115% of this optimum.

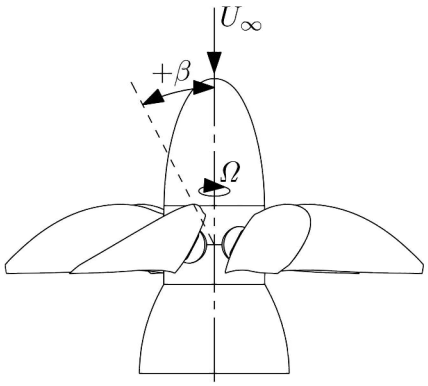

Figure 10: Definition of sideslip angle β (top view).

3 RESULTS

The results obtained from employment of the experimental methodology discussed in Chapter 2 are presented below. The data related to the pylon – pusher propeller interactions are treated in Sections 3.1 through 3.3, while the results focused on the swirl recovery vanes are discussed in Section 3.4.

3.1 Propeller Propulsive Performance

The propulsive performance data measured using the RSB were expressed in terms of the thrust coefficient C_T, torque coefficient C_Q, and propeller efficiency η, defined here as:

$$C_T = \frac{T}{\rho_\infty n^2 D^4} \quad (1) \qquad C_Q = \frac{Q}{\rho_\infty n^2 D^5} \quad (2) \qquad \eta = \frac{J}{2\pi}\frac{C_T \cos\beta}{C_Q} \quad (3)$$

with D the propeller diameter, J the propeller advance ratio ($J = U_\infty / nD$), n the propeller's rotational speed, Q the torque, T the thrust, and ρ_∞ the freestream density. Note that the thrust is expressed in the reference frame of the RSB and the in-plane components are neglected in the computation of the propeller efficiency.

The propulsive performance measured at zero sideslip was discussed elsewhere, and showed that in symmetric conditions the effect of pylon installation on the performance is negligible.[16] The effect of sideslip on the isolated propeller's propulsive performance is presented in Figure 11. To minimize the shift in the RSB's zero loading offset, the sideslip angle was changed at constant advance ratio.

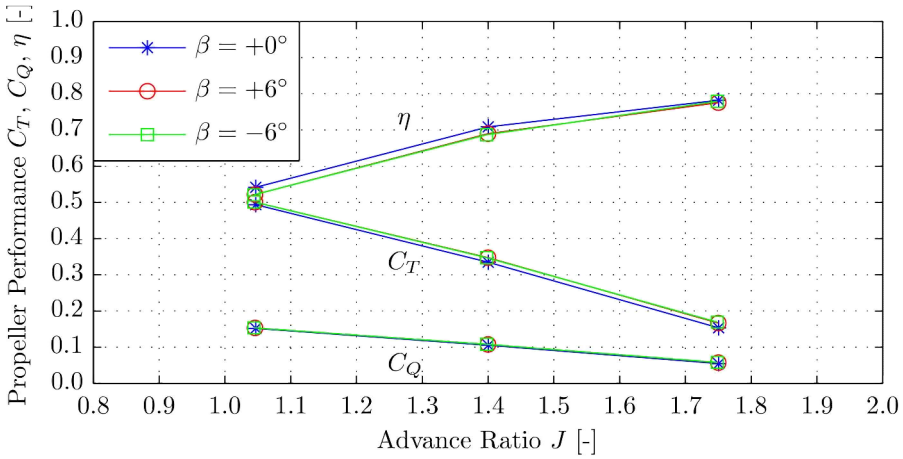

Figure 11: Effect of sideslip angle on propulsive performance of the isolated propeller.

Figure 11 shows that for the asymmetric configurations the periodic change in blade angle of attack increases the thrust compared to the symmetric configuration by about 1% at J = 1.05 up to 9% at J = 1.75. The rise in torque levels is smaller, with a maximum increase of around 5% at J = 1.75. The propeller efficiency defined by Eq. (3) is decreased by up to 3% at J = 1.75 compared to the results obtained for symmetric inflow conditions. The data measured at β = ±6° are the same due to the symmetry of the isolated propeller configuration.

Following the measurements of the isolated configuration, Figure 12 depicts the performance curves for the installed propeller at β = 0°, +6°, and −6°. These results were obtained in three different runs, in which the advance ratio was changed at constant sideslip angle. The error bars indicate the variability of repeated measurements, as computed from the multiple data points at constant operating conditions considered during the entire test program. At J = 1.05 the variation equaled 1%, increasing to 5% at J = 1.75. This was mainly due to shifts in the zero loading output of the balance.

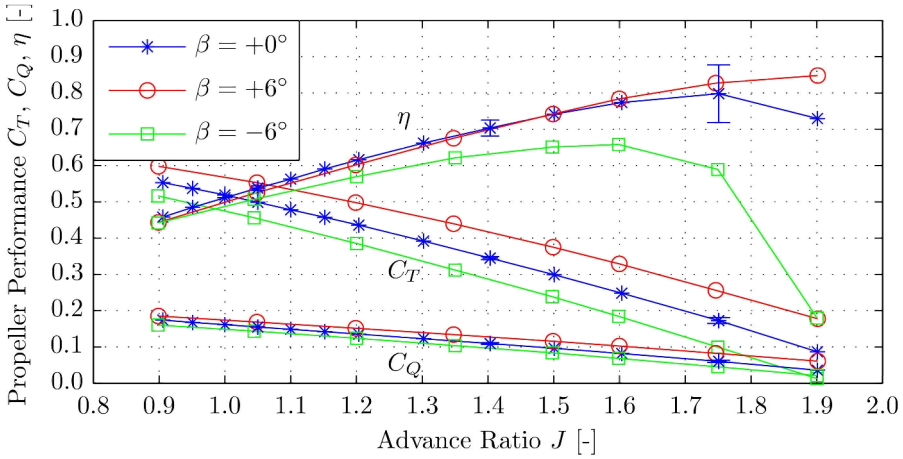

Figure 12: Effect of sideslip angle on propulsive performance of the installed propeller.

Figure 12 shows that the effect of the sideslip angle on the installed propulsive performance is significant. Compared to the symmetric configuration, at β = +6° the thrust is increased by 10% at J = 1.05 up to 45% at J = 1.75. At β = −6° on the other hand a reduction in thrust is observed of similar magnitude as the increase seen for β = +6°. This change in performance is attributed to pre-swirl effects: at β = +6° the sense of rotation of the pylon tip vortex was opposite to the rotation direction of the propeller. As a result, the blade angles of attack were increased, leading to increased thrust. For β = −6° the situation is reversed, with reduced local incidence angles, hence lower thrust. The absence of a dummy nacelle will have amplified the observed change in propeller performance due to the sideslip angle.

3.2 Pylon Wake Evaluations

Stereoscopic PIV measurements were performed to quantify the momentum deficit in the pylon wake, with and without pylon blowing. To facilitate comparisons between the measured wake profiles at a given streamwise position, an integral deficit parameter ξ is introduced as:

$$\xi = \int_{-b_w/R}^{+b_w/R} \left| 1 - \frac{U}{U_e} \right| \mathrm{d}\frac{Y}{R} \tag{4}$$

with b_w the wake half-width, R the propeller radius, U the local velocity in the wake region, U_e the velocity at the edge of the wake, and Y the lateral coordinate.

Figure 13 presents the mean velocity fields measured downstream of the pylon model in the unblown and blown configurations. Contours are plotted of the streamwise velocity component. The blown results were obtained at the optimal blowing coefficient of $c_{\dot{m}} = 1.6$.

The velocity fields displayed in Figure 13 show the momentum deficit in the wake region of the unblown pylon. Application of the blowing system indeed fills the pylon wake, thereby proving the effectiveness of the Uniform Blowing Rod. Whereas in the unblown configuration a maximum velocity deficit of about 20% of the freestream velocity is measured directly upstream of the propeller, at the optimal blowing rate the velocity in the wake center is recovered to the undisturbed value. Because of the small thickness of the blowing slit, the mixing between the blown and external flows is not optimal. As a result, some remaining velocity deficit is left in the blown wake. The velocity gradient outside of the pylon wake is due to the suction by the propeller.

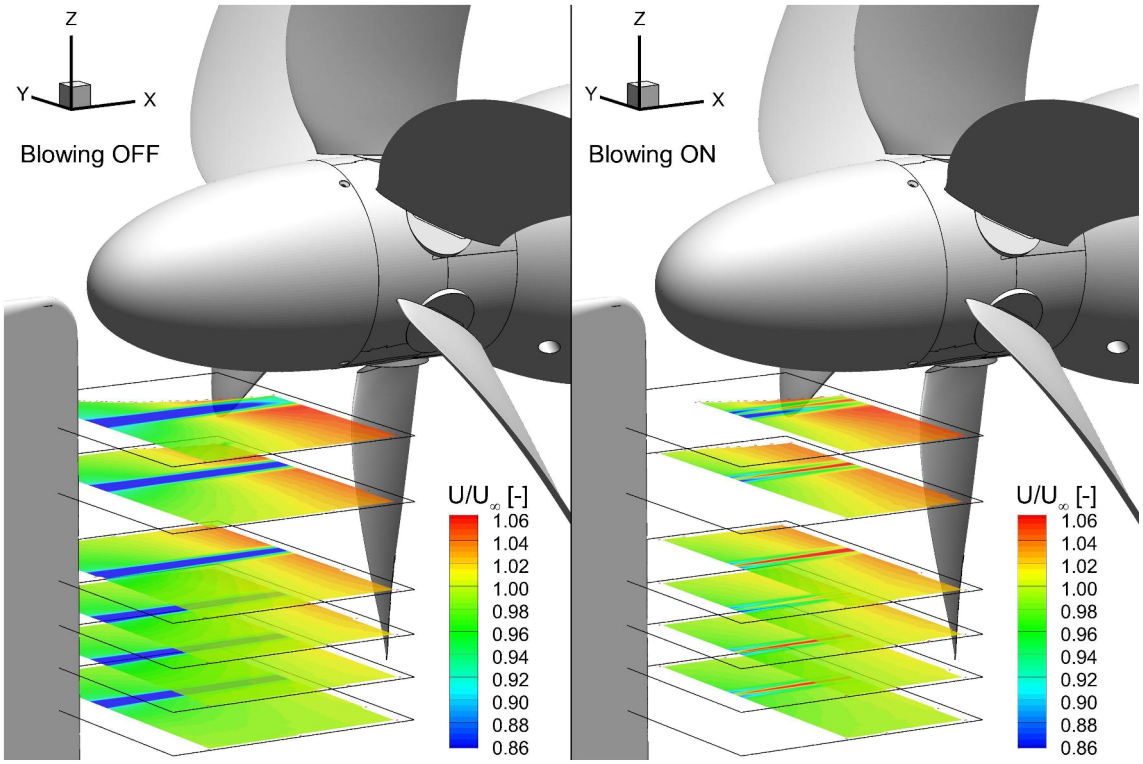

Figure 13: Pylon wake velocity fields with blowing off and on ($c_{\dot{m}} = 1.6$); $J = 1.4$, $\beta = 0°$.

Apart from the mean velocities, also the root mean square deviations of the instantaneous velocity components were assessed. These velocity fluctuations lead to additional propeller broadband noise emissions compared to the case without the pylon. Directly upstream of the propeller, in the unblown configuration the root mean square deviation of the axial velocity component equaled three to five percent of the freestream velocity. With blowing enabled this decreased to two to four percent.

To compare the pylon wake characteristics at different operating conditions, the integral velocity deficit in the pylon wake was computed following Equation (4). Figure 14 presents the results for the cases with and without blowing, as a function of advance ratio and measurement plane location. This location is expressed in terms of the radial coordinate of the downstream blade, when positioned in the wake center. The blown results were obtained at the optimal blowing coefficient.

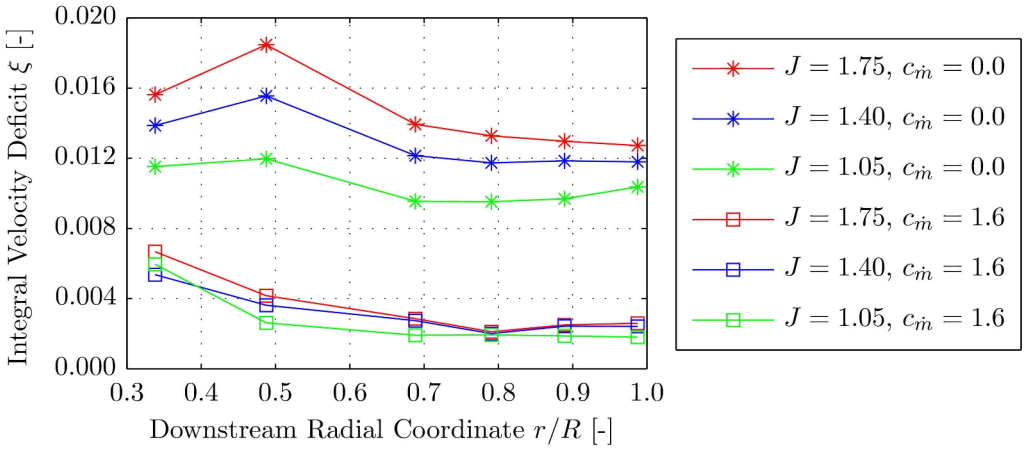

Figure 14: Integral velocity deficit versus advance ratio with blowing off and on; $\beta = 0°$.

Considering first the unblown case, Figure 14 shows that for $r/R > 0.6$ at constant advance ratio the integrated velocity deficit is approximately constant. The wake profiles upstream of the more inboard radial stations are characterized by a larger integral velocity deficit, due to three-dimensional tip effects and interactions with the spinner. The integrated velocity deficit in the pylon wake decreases with decreasing advance ratio. This is due to the favorable pressure gradient introduced by the suction of the propeller, which becomes stronger with increasing thrust setting. The change in wake characteristics with the propeller thrust setting is in contrast with a previous study, which found that the effect of the propeller on the pylon wake was negligible.[17]

The application of blowing at the optimal blowing coefficient reduces the momentum deficit in the pylon wake by 80%, except at the most inboard station for which the reduction is approximately 50%. The latter is due to the lower outflow velocity from the blowing system at this position.

3.3 Propeller Noise Emissions

Compared to the isolated propeller, with the pylon present the unsteady blade loads resulting from the local advance ratio reduction in the pylon wake lead to increased noise levels. Due to the cyclic occurrence of the pylon wake impingement, the additional noise is mainly of tonal nature, emitted at frequencies equal to multiples of the blade passage frequency (BPF). Additionally, the turbulence in the wake leads to an increase of the broadband noise levels. Figure 15 presents the sound spectra measured at a medium thrust setting for the configurations with and without the pylon. The effects of blowing are considered by including the results acquired at the optimal blowing coefficient. The data were obtained using the inflow microphones, at a position corresponding to an emission angle in the propeller plane (θ_e = 90°), perpendicular to the pylon (ϕ = 0°).

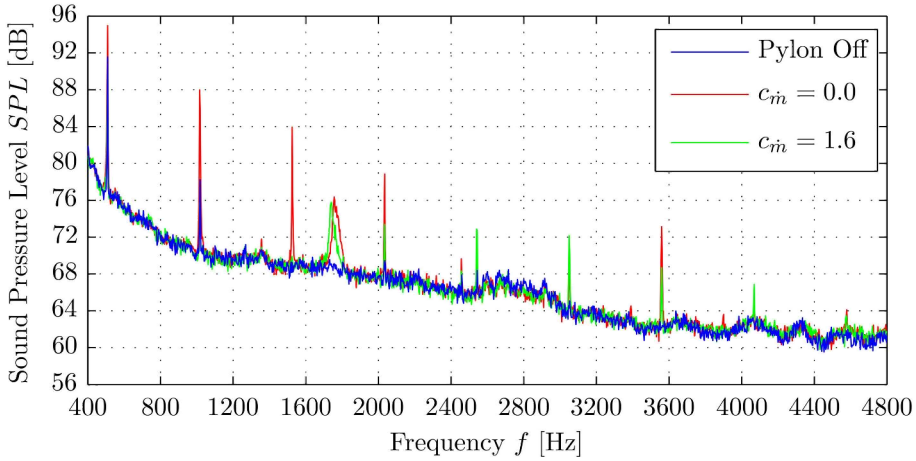

Figure 15: Sound spectra for the isolated and installed (with and without blowing) configurations; θ_e = 90°, ϕ = 0°, J = 1.40, β = 0°.

The sound spectra displayed in Figure 15 confirm the impact of the presence of the pylon on the propeller noise emissions. With the pylon installed, the SPL of the fundamental tone (f = 507 Hz) is increased by around 4 dB compared to the result measured for the isolated configuration. The levels of the harmonics are increased by up to 15 dB, however at sound pressure levels at least 7 dB lower than that of the fundamental tone. As discussed in Section 3.2, the application of pylon blowing reduces the velocity deficit in the pylon wake. Consequently, the amplitude of the unsteady blade loads during the wake passage is decreased. As shown in Figure 15, for the first three propeller tones this results in a recovery of the noise levels to the values measured for the isolated propeller. At higher frequencies the employment of blowing does not fully eliminate the installation penalty, which is due to the remaining non-uniformities in the blown pylon wake.

With the pylon installed, the tone observed at a frequency around 1,750 Hz is due to vortex shedding from the pylon trailing edge. This was confirmed by source localization performed using the DUT acoustic array, as shown in Figure 16.

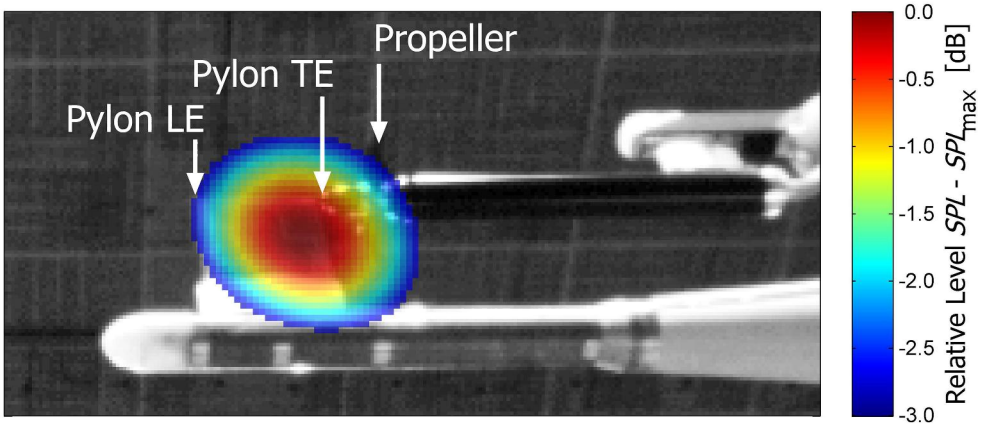

Figure 16: Source localization of pylon vortex shedding tone; $J = 1.40$, $\beta = 0°$, $c_m = 1.6$, 1,650 Hz < f < 1,800 Hz.

The directivity of the propeller noise emissions was evaluated by traversing the inflow acoustic instrumentation through the test hall in axial direction. A total tonal noise level was defined as the sum of the levels of the first eight propeller tones. Figure 17 displays this tonal noise level versus the axial directivity angle θ, for the isolated, unblown, and blown configurations.

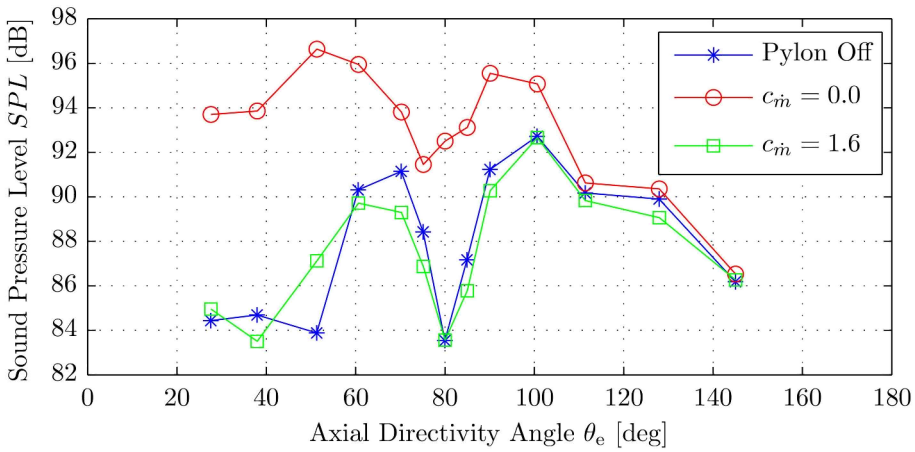

Figure 17: Axial directivity of summed tonal noise levels for the isolated and installed (with and without blowing) configurations; $\phi = 0°$, $J = 1.40$, $\beta = 0°$.

Figure 17 shows that installation of the pylon increases the noise levels over the entire axial directivity range. Compared to the sound pressure levels measured for the isolated configuration, an increase of up to 13 dB is observed. Application of pylon blowing eliminates the installation effects, and recovers the noise levels to those characteristic of the isolated propeller for all emission angles.

The directivity pattern of the isolated propeller's noise emissions displays an unexpected lobe around an emission angle of θ_e = 80°. The presence of this pattern is ascribed to aerodynamic interference effects with inflow support infrastructure, leading to an asymmetry in the propeller inflow. The resulting unsteady blade loads then introduce an additional noise generating mechanism, which interferes with the steady sources due to thickness and blade loading. This also explains the small differences between the isolated and installed noise levels around θ_e = 110° and further downstream.

3.4 Swirl Recovery Vanes

Following the evaluation of the propeller – pylon interactions, swirl recovery vanes were installed downstream of the isolated propeller. From the performance measurements using the RSB, which only measured the performance of the rotor, it was found that the upstream effect of the SRVs on the rotor performance is negligible. Over the entire advance ratio range considered the measured rotor thrust, torque, and efficiency were equal for the cases with and without the SRVs. This is as expected considering the small ratio of the total load generated by the vanes compared to the rotor, and the relatively large spacing between the rotor and the vanes.

The goal of installation of the SRVs is to convert the momentum associated with the swirl in the propeller slipstream into an additional axial momentum component, thereby increasing the thrust.[10] Since the shaft power remains unchanged, this increases the propulsive efficiency of the system. To assess the vanes' swirl recovery potential, the velocity in the propeller slipstream flow was measured using stereoscopic PIV, with and without the vanes installed. A swirl kinetic energy ratio was introduced as the fraction of the kinetic energy of the swirl and freestream axial components:

$$\frac{E_k^{\text{swirl}}}{E_k^{\infty}} = \frac{V^2 + W^2}{U_{\infty}^2} \tag{5}$$

with U, V, and W the axial, lateral, and vertical velocity components. Figure 18 displays contours of the swirl kinetic energy ratio defined by Equation (5) measured with and without the swirl recovery vanes, at a high thrust setting ($J = 1.05$).

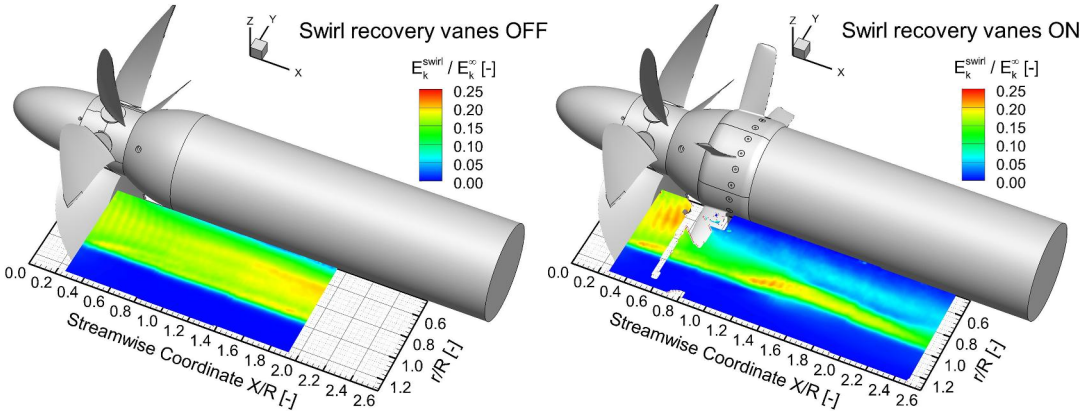

Figure 18: Swirl recovery due to installation of the swirl recovery vanes; $J = 1.05$, $\beta = 0°$.

Figure 18 displays that installation of the SRVs reduces the swirl kinetic energy compared to the isolated configuration. The swirl is decreased by 50% when considering the average reduction in radial direction at a position one propeller radius downstream of the propeller. The largest reductions are achieved downstream of the inboard part of the blade, while near the edge of the slipstream the flow field is unchanged because of the 90% crop of the SRV diameter. Although Figure 18 confirms the efficacy of the SRVs in reducing the swirl in the slipstream of the isolated propeller, it does not evidence that the presence of the vanes increased the propulsive efficiency of the system. Since the SRVs were not instrumented, it was not possible to determine their contribution to the total thrust.

Compared to the isolated propeller, the installation of the vanes introduces two additional noise generating mechanisms. The periodic impingement of the rotor blade wakes and possible tip vortices on the vanes leads to unsteady forces on the SRVs, hence additional noise emissions. Moreover, the presence of the vanes introduces upstream potential effects, causing unsteady rotor blade loading. Since the vanes are stationary, the additional noise will be generated at frequencies equal to

multiples of the rotor's BPF. The noise penalty due to installation of the SRVs was assessed by comparing the inflow microphone data measured for the configurations with and without the vanes. Figure 19 presents the sound spectra acquired at an emission angle of θ_e = 90° (in the propeller plane), at a relatively high thrust setting (J = 1.05). The sound pressure levels are plotted versus the frequency, expressed as multiples of the rotor BPF. For the operating point considered in Figure 19, the BPF equals 677 Hz. The part of the spectrum corresponding to frequencies below the fundamental tone is omitted because of the dominance of irrelevant wind tunnel and background noise components.

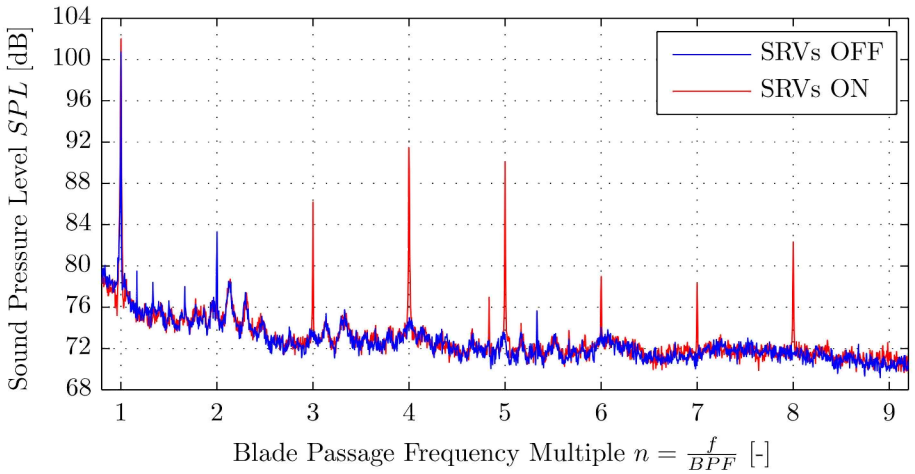

Figure 19: Sound spectra for the isolated propeller with (SRVs ON) and without (SRVs OFF) swirl recovery vanes; θ_e = 90°, ϕ = 0°, J = 1.05, β = 0°, BPF = 677 Hz.

Figure 19 shows that, both with and without the SRVs present, the noise emissions of the propulsion system are dominated by the fundamental tone (1BPF). Installation of the SRVs increases the amplitude of this tone by 1 dB. At higher frequencies the tonal noise emissions are affected much more strongly by installation of the vanes, with noise increases of up to 20 dB. Summed over all measured tones, the SPL increased by 2 dB due to installation of the vanes. This noise penalty is the result of the upstream and downstream interactions discussed earlier. Considering the small impact of the installation of the vanes on the rotor performance, it is expected that the contribution of the upstream mechanism is small. To confirm this, Figure 20 presents the acoustic array result obtained for the case with the SRVs present, for the same operating point as considered in Figure 19. The analyzed frequency range was centered around a frequency of four times the BPF.

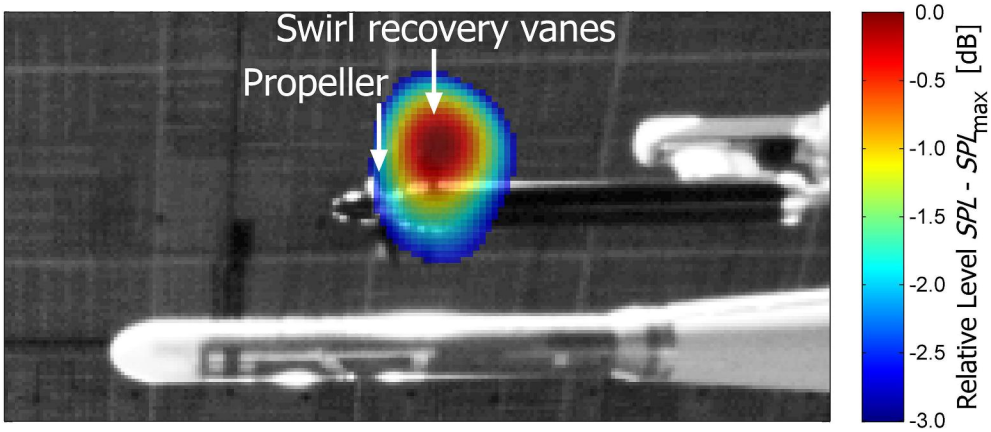

Figure 20: Source localization of noise emissions with swirl recovery vanes installed; J = 1.05, β = 0°, 2,680 Hz < f < 2,730 Hz.

The acoustic array result depicted in Figure 20 confirms that the tonal noise component observed at a frequency of four times the rotor BPF indeed originates from the SRVs. Similar results were obtained for the frequency ranges around the other tonal components shown in the sound spectrum, but are not presented here. Consequently, it is concluded that the downstream interaction is dominant, and the upstream effect of the SRVs on the rotor is negligible. Analysis of the PIV data showed that the 90% crop of the SRV diameter was sufficient to prevent the impingement of the rotor tip vortices on the vanes, hence the downstream interaction was due to rotor blade wake impingement only.

4 CONCLUSIONS

An experimental investigation was performed to study pusher propeller – pylon interaction effects, with and without pylon blowing. Also, a preliminary assessment of the aerodynamic and aeroacoustic impact of swirl recovery vanes downstream of the isolated propeller was performed. From the measurements of the pylon installation effects it was concluded that:

- The effect of pylon installation on the propulsive performance is only significant in asymmetric inflow conditions. At a sideslip angle of +6° the sense of rotation of the pylon tip vortex was opposite to the rotation direction of the propeller, leading to a thrust increase of 10% at a high thrust setting up to 45% for a low thrust condition. The fact that no dummy nacelle was installed in the test setup will have amplified the measured change in performance.
- Pylon blowing can successfully be employed to fill the momentum deficit in the pylon wake. In the present study, a reduction in integrated velocity deficit of 80% was obtained compared to the unblown case. The blowing system based on the uniform blowing rod has shown to be an effective design while maintaining a simple geometrical layout.
- Installation of the pylon upstream of the propeller strongly increases the noise emissions. At a medium thrust setting, the tonal noise level increased by up to 13 dB due to the presence of the pylon. Application of the blowing system eliminated this installation penalty, by bringing the noise levels back to the values recorded for the isolated propeller.

The measurements performed with the swirl recovery vanes mounted downstream of the isolated propeller led to the following conclusions:

- Installation of the swirl recovery vanes reduces the kinetic energy of the swirl components in the propeller slipstream. At a high thrust setting, an integral swirl recovery of 50% was achieved. The rotor performance was not affected by the presence of the vanes.
- Compared to the isolated propeller, installation of the vanes mainly increases the noise levels of the propeller harmonics. The summed tonal noise level with SRVs installed was 2 dB higher than without the vanes. Source localization using an acoustic array substantiated that the additional noise originated from the vanes, thereby confirming that the upstream effect of the vanes on the rotor is negligible.

5 ACKNOWLEDGEMENTS

The results presented in this paper were obtained by the APIAN-INF research partners in the framework of the transnational access program organized by the ESWIRP consortium, as part of the ESWIRP project (European Strategic Wind tunnels Improved Research Potential). The research leading to these results has received funding from the European Union Seventh Framework Programme (FP7-INFRASTRUCTURE-2008-1) under grant agreement n° 227816.

The authors would like to thank Kyle P. Lynch for his crucial contributions to the preparation, acquisition, processing, and analysis of the PIV measurements.

6 REFERENCES

[1] S. A. E. Mann, C. A. Stuart, *Advanced propulsion through the 1990s - An Airframers View*, 21st AIAA/SAE/ASME/ASEE Joint Propulsion Conference, Monterey, CA, USA, 1985.

[2] A. Stürmer, J. Yin, *Aerodynamic and Aeroacoustic Installation Effects for Pusher Configuration CROR Propulsion Systems*, 28th AIAA Applied Aerodynamics Conference, Chicago, IL, USA, 2010.

[3] B. Shivishankara, D. Johnson, R. Cuthbertson, *Installation Effects on Counter Rotating Propeller Noise*, 13th AIAA Aeroacoustics Conference, Tallahassee, FL, USA, 1990.

[4] J. Ricouard, E. Julliard, M. Omaïs, V. Regnier, A. B. Parry, S. Baralon, *Installation effects on contra-rotating open rotor noise*, 16th AIAA/CEAS Aeroacoustics Conference, Stockholm, Sweden, 2010.

[5] C. Paquet, E. Julliard, N. Genoulaz, J. Ricouard, P. Spiegel, *Z08: low-speed aero-acoustic experimental characterization of open rotor installation on aircraft*, 20th AIAA/CEAS Aeroacoustics Conference, Atlanta, GA, USA, 2014.

[6] G. L. Gentry Jr., E. R. Booth Jr., M. A. Takallu, *Effect of Pylon Wake With and Without Pylon Blowing on Propeller Thrust*, NASA-TM-4162, 1990.

[7] T. Sinnige, L. L. M. Veldhuis, *Pylon Trailing Edge Blowing Effects on the Performance and Noise Production of a Pusher Propeller*, 52nd Aerospace Sciences Meeting, National Harbor, MD, USA, 2014.

[8] R. Fernando, M. Leroux, *Open-Rotor low speed aero-acoustics: wind tunnel characterization of an advanced blade design in isolated and installed configurations*, 20th AIAA/CEAS Aeroacoustics Conference, Atlanta, GA, USA, 2014.

[9] A. Stürmer, J. Yin, *Pylon Trailing Edge Blowing for the Control of CROR Unsteady Blade Loads*, "New Results in Numerical and Experimental Fluid Mechanics VIII", edited by A. Dillmann, G. Heller, H.-P. Kreplin, W. Nitsche, I. Peltzer, Vol. 121 of Notes on Numerical Fluid Mechanics and Multidisciplinary Design, pp. 715-722, Springer Berlin Heidelberg, 2013.

[10] J. Gazzaniga, G. Rose, *Wind tunnel performance results of swirl recovery vanes as tested with an advanced high speed propeller*, 28th Joint Propulsion Conference & Exhibit, Nashville, TN, USA, 1992.

[11] J. H. Dittmar, D. G. Hall, *Cruise Noise of an Advanced Propeller with Swirl Recovery Vanes*, Journal of Aircraft, Vol. 30, No. 2, pp. 221-226, 1993.

[12] P. Crozier, *APIAN Installed Tests in the ONERA S1MA Wind Tunnel*, 39th AIAA Aerospace Sciences Meeting & Exhibit, Reno, NV, USA, 2001.

[13] I. Philipsen, H. Hoeijmakers, S. Hegen, *An Overview of Advanced Propeller Simulation Tests in the German Dutch Wind Tunnels (DNW)*, 22nd AIAA Aerodynamic Measurement Technology and Ground Testing Conference, St. Louis, MO, USA, 2002.

[14] M. Drela, H. Youngren, *XROTOR: an interactive program for the design and analysis of ducted and free-tip propellers and windmills*, 2011. Available at http://web.mit.edu/drela/Public/web/xrotor, accessed 13 November 2014.

[15] P. Sijtsma, *Acoustic beamforming for the ranking of aircraft noise*, National Aerospace Laboratory NLR -TP-2012-137, 2012.

[16] T. Sinnige, K. P. Lynch, D. Ragni, G. Eitelberg, L. L. M. Veldhuis, *Aerodynamic and Aeroacoustic Effects of Pylon Trailing Edge Blowing on Pusher Propeller Installation*, 21st AIAA/CEAS Aeroacoustics Conference, Dallas, TX, USA, 2015.

[17] W. C. Horne, P. T. Soderman, *Flow-Field Survey of an Empennage Wake Interacting with a Pusher Propeller*, NASA-TM-101003, 1988.